srGAP1 regulates lamellipodial dynamics and cell migratory behavior by modulating Rac1 activity

Daisuke Yamazaki[a,b], Toshiki Itoh[a], Hiroaki Miki[b], and Tadaomi Takenawa[c]
[a]Division of Membrane Biology and [c]Laboratory of Lipid Biochemistry, Department of Biochemistry and Molecular Biology, Kobe University Graduate School of Medicine, 7-5-1 Kusunoki-cho, Chuo-ku, Kobe 650-0017, Japan;
[b]Department of Cellular Regulation, Research Institute for Microbial Diseases, Osaka University, 3-1 Yamadaoka, Suita, Osaka 565-0871, Japan

ABSTRACT **The distinct levels of Rac activity differentially regulate the pattern of intrinsic cell migration. However, it remains unknown how Rac activity is modulated and how the level of Rac activity controls cell migratory behavior. Here we show that Slit-Robo GAP 1 (srGAP1) is a modulator of Rac activity in locomotive cells. srGAP1 possesses a GAP activity specific to Rac1 and is recruited to lamellipodia in a Rac1-dependent manner. srGAP1 limits Rac1 activity and allows concomitant activation of Rac1 and RhoA, which are mutually inhibitory. When both GTPases are activated, the protrusive structures caused by Rac1-dependent actin reorganization are spatially restricted and periodically destabilized, causing ruffling by RhoA-induced actomyosin contractility. Depletion of srGAP1 overactivates Rac1 and inactivates RhoA, resulting in continuous spatiotemporal spreading of lamellipodia and a modal shift of intrinsic cell motility from random to directionally persistent. Thus srGAP1 is a key determinant of lamellipodial dynamics and cell migratory behavior.**

Monitoring Editor
Asma Nusrat
Emory University

Received: Apr 4, 2013
Revised: Aug 12, 2013
Accepted: Aug 29, 2013

INTRODUCTION

Cell migration plays a pivotal role in various biological processes, including tissue morphogenesis and tumor metastasis. The sheet-like membrane protrusions observed at the leading edge of locomotive cells are the lamellipodia, and their formation is the first step in cell migration (Pollard and Borisy, 2003; Ridley *et al.*, 2003). The number, extent, and direction of lamellipodia dynamically vary, and changes correlate well with the speed and direction of cell migration (Petrie *et al.*, 2009). Therefore it is important to understand the molecular mechanisms involved in the control of lamellipodial dynamics.

Rac plays a central role in the control of membrane protrusions termed lamellipodia at the front of locomotive cells (Ridley, 2011). Activated Rac1 induces actin polymerization through the WAVE/Arp2/3 complex (Miki *et al.*, 2000; Yamazaki *et al.*, 2003; Takenawa and Suetsugu, 2007) and promotes membrane protrusions (Wu *et al.*, 2009). Rac level determines cell migratory behavior through control of the number and stability of lamellipodial protrusions, and activation that is too low or too high leads to immobilization (Pankov *et al.*, 2005). Thus spatiotemporal activation of Rac must be tightly regulated. In addition to Rac, Rho is also a key player in the regulation of lamellipodial dynamics (Pertz, 2010; Ridley, 2011). At lamellipodia RhoA might be involved in mDia-dependent actin polymerization (Kurokawa and Matsuda, 2005; Sarmiento *et al.*, 2008), but its significance is controversial. Lamellipodial extensions are normally followed by membrane ruffling and retraction (Small and Resch, 2005), which is cooperatively regulated by Rac1 and RhoA (Kurokawa and Matsuda, 2005; Pertz *et al.*, 2006; Machacek *et al.*, 2009). There is functional antagonism between Rac1 and RhoA (Malliri and Collard, 2003; Burridge and Wennerberg, 2004), and overactivated Rac1 can suppress the function of RhoA (Kurokawa and Matsuda, 2005; Pertz *et al.*, 2006; Wu *et al.*, 2009). Therefore their activities are spatiotemporally coordinated to accomplish membrane dynamics at the lamellipodia (Machacek *et al.*, 2009). However, the molecular mechanisms modulating the activities of the two GTPases at lamellipodia and their subsequent control of lamellipodial dynamics remain unknown.

This article was published online ahead of print in MBoC in Press (http://www.molbiolcell.org/cgi/doi/10.1091/mbc.E13-04-0178) on September 4, 2013.
Address correspondence to: Daisuke Yamazaki (dayama@biken.osaka-u.ac.jp)
Abbreviations used: CT, carboxyl-terminal; FRET, fluorescence resonance energy transfer; MRLC, myosin regulatory light chain; RNAi, RNA interference; siRNA, small interfering RNA; srGAP, Slit-Robo GAP.

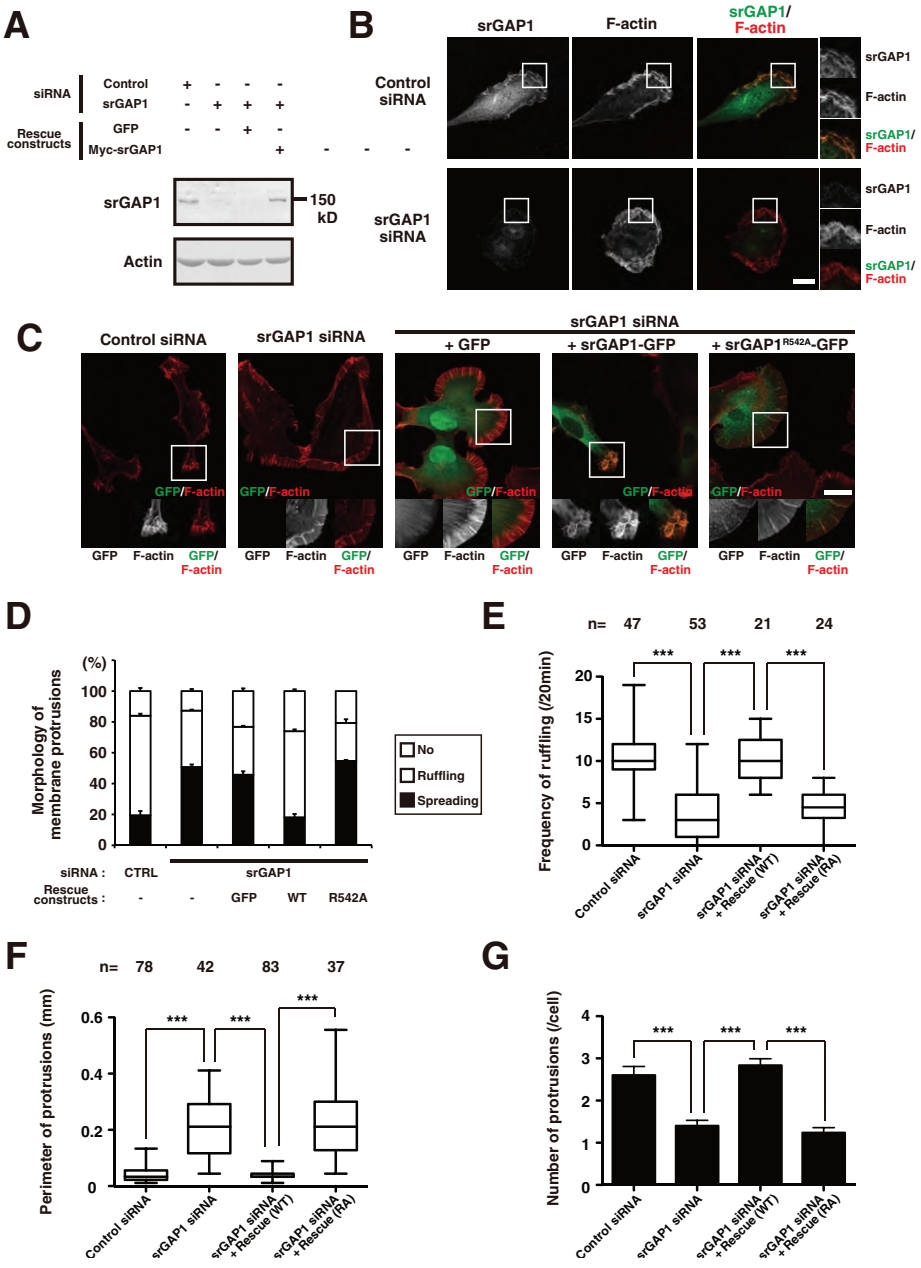

FIGURE 1: srGAP1 regulates the properties of the sheet-like membrane protrusions. (A) Western blot analysis of HT1080 cells transfected with the indicated siRNAs and the rescue constructs. (B) Cells treated with the indicated siRNAs were stained for srGAP1 (green) and actin filament (F-actin; red). Magnified images of the areas indicated by the white squares. Scale bar, 20 μm. (C) Morphologies of srGAP1-depleted cells. Cells transfected with the indicated siRNAs and the GFP-fused rescue constructs (green) were stained for F-actin (red). Magnified images of the boxed areas indicated by the white squares (left, GFP; middle, F-actin; right, merged). Scale bar, 20 μm. (D) Quantification of the morphologies of sheet-like membrane protrusions. Cells transfected with the indicated siRNAs and rescue constructs were stained for F-actin. Cells were classified on the basis of morphology of the membrane protrusion. Cells more than half of whose protrusive area was ruffling were considered ruffling. Cells more than half of whose protrusive area was spreading were considered spreading. Cells without the sheet-like membrane protrusions were considered no. We analyzed 150 cells from three independent experiments. Error bars indicate SEM. (E) Quantification of the frequency of membrane ruffling. We counted the number of rufflings of the largest membrane protrusions in each cell for 20 min. Three independent experiments were performed. The total number of analyzed cells is shown above each bar. Error bars indicate SEM. $^{**}p < 0.01$, $^{***}p < 0.001$. (F) Quantification of the perimeter of the sheet-like membrane protrusions. The total number of analyzed protrusions is shown above each bar. Error bars indicate SEM. $^{**}p < 0.01$, $^{***}p < 0.001$. (G) Quantification of the number of sheet-like membrane protrusions. Thirty cells were analyzed from three independent experiments. Error bars indicate SEM. $^{**}p < 0.01$, $^{***}p < 0.001$.

Slit-Robo GAP (srGAP) functions as a GAP for Rho-family GTPases downstream of Slit-Robo signaling (Wong *et al.*, 2001). srGAP is composed of three functional domains—F-BAR (Itoh *et al.*, 2005; Tsujita *et al.*, 2006), RhoGAP, and SH3—and one functionally unknown carboxyl-terminal (CT) region (Tcherkezian and Lamarche-Vane, 2007). In mammals, four structurally similar proteins have been identified, namely, srGAP1, srGAP2, srGAP3/WRP, and ARHGAP4/p115 (Wong *et al.*, 2001; Tcherkezian and Lamarche-Vane, 2007). srGAP2, srGAP3, and ARHGAP4 have GAP activity for Rac (Foletta *et al.*, 2002; Soderling *et al.*, 2002; Yang *et al.*, 2006; Guerrier *et al.*, 2009; Mason *et al.*, 2011), and the nematode orthologue of srGAP1, SRGP-1, possesses GAP activity for CED-10, the nematode orthologue of Rac1 (Neukomm *et al.*, 2011), suggesting that srGAPs regulate Rac activity. srGAP2, srGAP3, and ARHGAP4 localize to the leading edge and negatively regulate cell migration (Yang *et al.*, 2006; Vogt *et al.*, 2007; Guo and Bao, 2010; Endris *et al.*, 2011; Mason *et al.*, 2011). Of interest, these GAPs interact with the regulatory molecules of actin reorganization at the cell periphery (Soderling *et al.*, 2002; Weiner *et al.*, 2006; Endris *et al.*, 2011; Mason *et al.*, 2011), which suggests their involvement in the control of lamellipodial protrusions. However, the role of srGAPs as RacGAPs in the control of the lamellipodial dynamics and cell migration is largely unknown.

In this study, we show that srGAP1 modulates Rac1 activity via its RacGAP activity, resulting in concomitant activation of Rac1 and RhoA at lamellipodia. These findings are important, as the coordination of their activities is crucial for control of lamellipodial dynamics and cell migratory behavior.

RESULTS

srGAP1 regulates the dynamics of lamellipodial protrusions

Immunostaining revealed that endogenous srGAP1 is localized to the tip of the ruffling membranes in HT1080 fibrosarcoma cells (Figure 1, A and B). To examine the role of srGAP1 in the control of lamellipodia, we repressed its expression by RNA interference (RNAi) in HT1080 cells (Figure 1A).

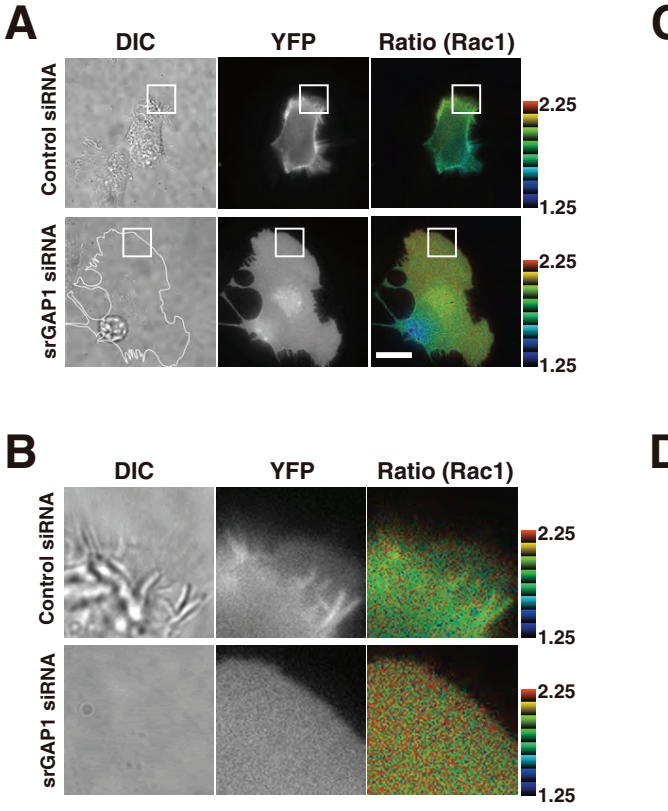

FIGURE 2: Imaging of Rac1 activity. (A–D) HT1080 cells were treated with the indicated siRNAs and then transfected with FRET probes for Rac1. Cells were imaged for YFP, CFP, and differential interference contrast (DIC) every 20 s for 20 min. FRET efficiencies are shown as YFP/CFP ratio images. White line is an outline of an srGAP1-depleted cell. (B) Magnified images of the boxed areas in A. Scale bar, 20 μm. (C, D) Emission ratio of YFP/CFP was measured for the entire region (C) and the membrane protrusions of the cells (D) using MetaMorph software. The total number of analyzed cells is shown above each bar. Three independent experiments were performed. Error bars indicate SEM. *$p < 0.05$, **$p < 0.01$.

Depletion of srGAP1 did not affect the ratio of cells with lamellipodial protrusions but altered their morphology (Figure 1, C and D). When treated with the control small interfering RNA (siRNA), 60% of cells showed ruffling membranes and 20% had spreading membranes. In the srGAP1-depleted cells, the relative number of cells with ruffling membranes decreased and the number of cells with spreading membranes increased in comparison with control cells (Figure 1D). To analyze such morphological differences in more detail, we observed the dynamics of membrane protrusions by time-lapse imaging using phase-contrast microscopy and analyzed them by kymography, which produces a time line of protrusion and retraction. In control cells with ruffling membranes, membrane extension was interrupted by ruffling of the membrane followed by retraction (Supplemental Figure S1A and Supplemental Movie S1). The cycle, which was composed of ruffling and retraction of the membrane protrusions, was continuously and periodically repeated, thereby resulting in the ruffling structure of the lamellipodia in the HT1080 cells. Depletion of srGAP1 decreased the frequency of membrane ruffling and increased the persistence of membrane extension, which resulted in the spreading structure of lamellipodia with less ruffling (Figure 1E, Supplemental Figure S1B, and Supplemental Movie S2). Thus the spreading morphology of protrusions is due to decreased ruffling in srGAP1-depleted cells.

In addition to repressed ruffling, the width of each protrusion was larger after srGAP1 depletion (Figure 1C). Indeed, the perimeter of each protrusion confirmed the significant difference between the cells (Figure 1F). Furthermore, the number of protrusions per cell was greater in control than in srGAP1-depleted cells (Figure 1G). Of importance, such morphological changes in lamellipodial protrusions were also observed in the cells treated with two additional siRNAs directed against srGAP1 (Supplemental Figure S2). Thus srGAP1 is involved in the control of the number, size, and dynamics of lamellipodia.

srGAP1 regulates Rac1 activity at lamellipodial protrusions

To examine the importance of the GAP activity of srGAP1 in the regulation of lamellipodia, we generated a GAP activity–deficient mutant of srGAP1 by substituting the conserved arginine in the GAP domain to alanine (srGAP1^{R542A}; Bos *et al.*, 2007). Ectopic expression of srGAP1 reduced the amount of active Rac1 but not RhoA and Cdc42 in COS7 cells (Supplemental Figure S3A). However, the Rac1 activity was not affected in srGAP1^{R542}-expressing cells. In addition, a recombinant srGAP1 decreased the amount of active Rac1 in vitro (Supplemental Figure S3, B and C). Thus srGAP1, in addition to srGAP2 and srGAP3, functions as a RacGAP, which is expected, considering that the GAP domains of these proteins are highly similar (77.7% identity between srGAP1 and srGAP2 and 79.3% identity between srGAP1 and srGAP3; Soderling *et al.*, 2002; Guerrier *et al.*, 2009). Rescue experiments were performed in which the srGAP1 construct resistant to the srGAP1 siRNA (Figure 1A) was expressed in cells treated with srGAP1 siRNA. Reexpression of srGAP1, but not of srGAP1^{R542A}, restored the ruffling, perimeter, and number of lamellipodial protrusions (Figure 1, C–G, and Supplemental Figure S1, C and D). Thus srGAP1 regulates lamellipodial dynamics in a GAP activity–dependent manner.

Next the cellular Rac1 activity was imaged with Raichu-Rac1, which is a based on the principle of the fluorescence resonance energy transfer (FRET) probe (Itoh *et al.*, 2002). In control cells, Rac1 activity increased toward the membrane protrusions (Figure 2A), and Rac1 activity at the membrane did not change during the extension–retraction cycle (Supplemental Figure S4). Although Rac1 activity increased toward the lamellipodia also in srGAP1-depleted cells (Figure 2A), srGAP1 depletion significantly increased Rac1 activity not only at lamellipodia, but also in the total cell area (Figure 2, A–D). Reexpression of srGAP1 repressed the increase and propagation of Rac1 activity caused by srGAP1 depletion (Figure 2, C and D). Thus srGAP1 inhibits excessive activation of Rac1 at lamellipodial protrusions and its propagation throughout the cell.

To confirm whether changes in the properties of the membrane protrusions in srGAP1-depleted cells were due to increased Rac1 activity, Rac1 we also repressed expression by RNAi (Figure 3A). The partial repression of Rac1 expression by treatment with 0.1 nM Rac1 siRNA recovered membrane ruffling in srGAP1-depleted cells (Figure 3, B and C). Conversely, expression of a constitutively active

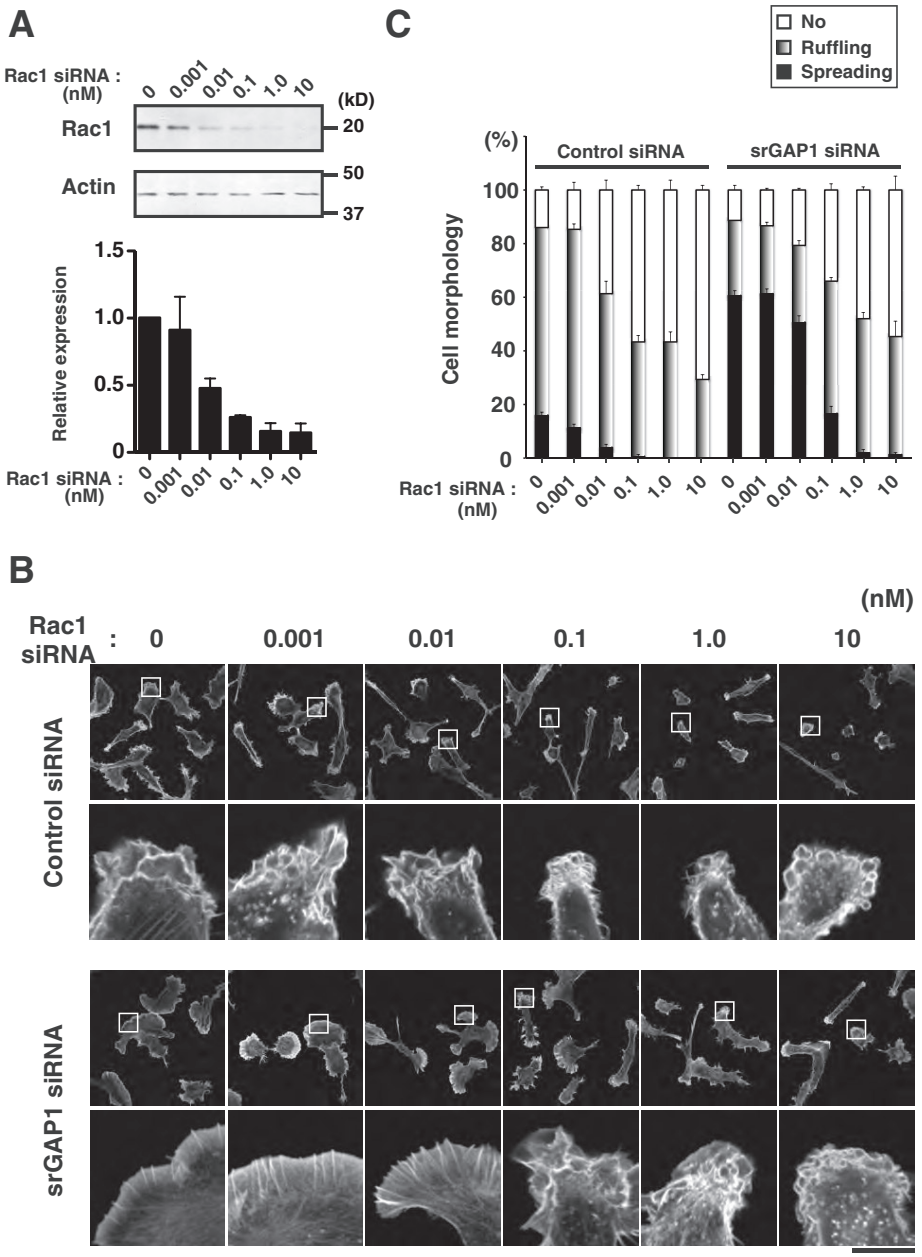

FIGURE 3: Partial depletion of Rac1 recovers membrane ruffling in srGAP1-depleted cells. (A) Western blot analysis of cells treated with the indicated amounts of Rac1 siRNA. Signal intensity of Rac1 was quantified with ImageJ. The amounts of Rac1 were normalized to those of actin. In the graphs, the amount of Rac1 in cells treated with Rac1 siRNA is normalized to that in nontreated cells. Three independent experiments were performed. Error bars indicate SEM. (B) Cells were treated with control or srGAP1 siRNAs and then with the indicated amounts of Rac1 siRNA after 24 h of the first treatment. After 24 h of the second treatment cells were fixed and stained for F-actin. Bottom, magnified images of the boxed areas in the top. Scale bar, 100 μm (top) and 12.5 μm (bottom). (C) Quantification. Morphologies of the sheet-like membrane protrusions classified as described in Figure 1D. From three independent experiments, 150 cells were analyzed. Error bars indicate SEM.

mutant of Rac1 ($Rac1^{G12V}$) showed the same effect on lamellipodial protrusions as srGAP1 depletion (Supplemental Figure S5). Furthermore, activation of Rac1 promoted spreading of the protrusions more effectively than that of RhoA and Cdc42 in HT1080 cells (Supplemental Figure S6). These results suggest that srGAP1-dependent regulation of Rac1 activity is important for the control of lamellipodia.

Rac1 signaling regulates recruitment of srGAP1 to the membrane through the F-BAR–FX unit

To examine the spatial regulation of srGAP1, we ectopically expressed it and observed its cellular localization in COS7 cells. Exogenous srGAP1 showed cytosolic distribution, but the GAP-dead and GAP-deleted mutants (R542A and ΔGAP, respectively) of srGAP1 were localized to the tip of the membrane protrusions (Supplemental Figure S7). These results suggest that GAP-dependent inactivation of endogenous Rac disrupts the membrane localization of srGAP1. Of importance, $Rac1^{G12V}$ expression dramatically increased membrane localization of srGAP1 (Figure 4, A and B). Thus Rac1 signaling is important for membrane recruitment of srGAP1.

Next, to further investigate the mechanisms by which Rac1 signaling recruits srGAP1 to the membrane, we expressed the various deletion constructs of srGAP1 with $Rac1^{G12V}$ and examined their localizations. The N-terminal 500 amino acids of srGAP2 and srGAP3 were recognized as one functional domain (Guerrier *et al.*, 2009; Carlson *et al.*, 2011; Endris *et al.*, 2011; Coutinho-Budd *et al.*, 2012). We found that this region is separated into two lipid-binding domains, namely, F-BAR and FX, as well as Fer and Fes (Itoh *et al.*, 2009; Figure 4C). It was reported that expression of the F-BAR–FX unit of srGAP2 and srGAP3 can induce filopodia-like plasma membrane protrusions (Guerrier *et al.*, 2009; Carlson *et al.*, 2011; Endris *et al.*, 2011; Coutinho-Budd *et al.*, 2012): however, our study determined that the F-BAR–FX unit of srGAP1 could not induce such membrane deformations as well as that of srGAP2 (Supplemental Figure S8), as described previously (Coutinho-Budd *et al.*, 2012). Thus the properties of the F-BAR–FX unit of srGAP1 are distinct from those of the other srGAPs. Of interest, deletion of the F-BAR and/or FX domains abrogated the Rac1-induced membrane localization of srGAP1, and the F-BAR–FX unit alone was recruited to the membrane (Figure 4, D and E). The signal intensity of the F-BAR–FX unit at the membrane was increased by coexpression of $Rac1^{G12V}$ and decreased by the Rac1 dominant-negative mutant ($Rac1^{T17N}$; Figure 4, A and B). Besides the F-BAR–FX unit, the CT region is needed for Rac1-induced membrane localization of srGAP1 (Figure 4, D and E).

The BAR domain, which is structurally similar to the F-BAR domain, binds with both acidic phospholipids and small GTPases (Habermann, 2004; de Kreuk *et al.*, 2011). Indeed, each of the F-BAR and FX domains of srGAP1 possesses lipid-binding activity (Figure 5A). The F-BAR domain of srGAP1 directly interacts with Rac1, and the affinity between both proteins increases in a manner dependent on Rac1 activity (Figure 5, B–D), suggesting the importance of

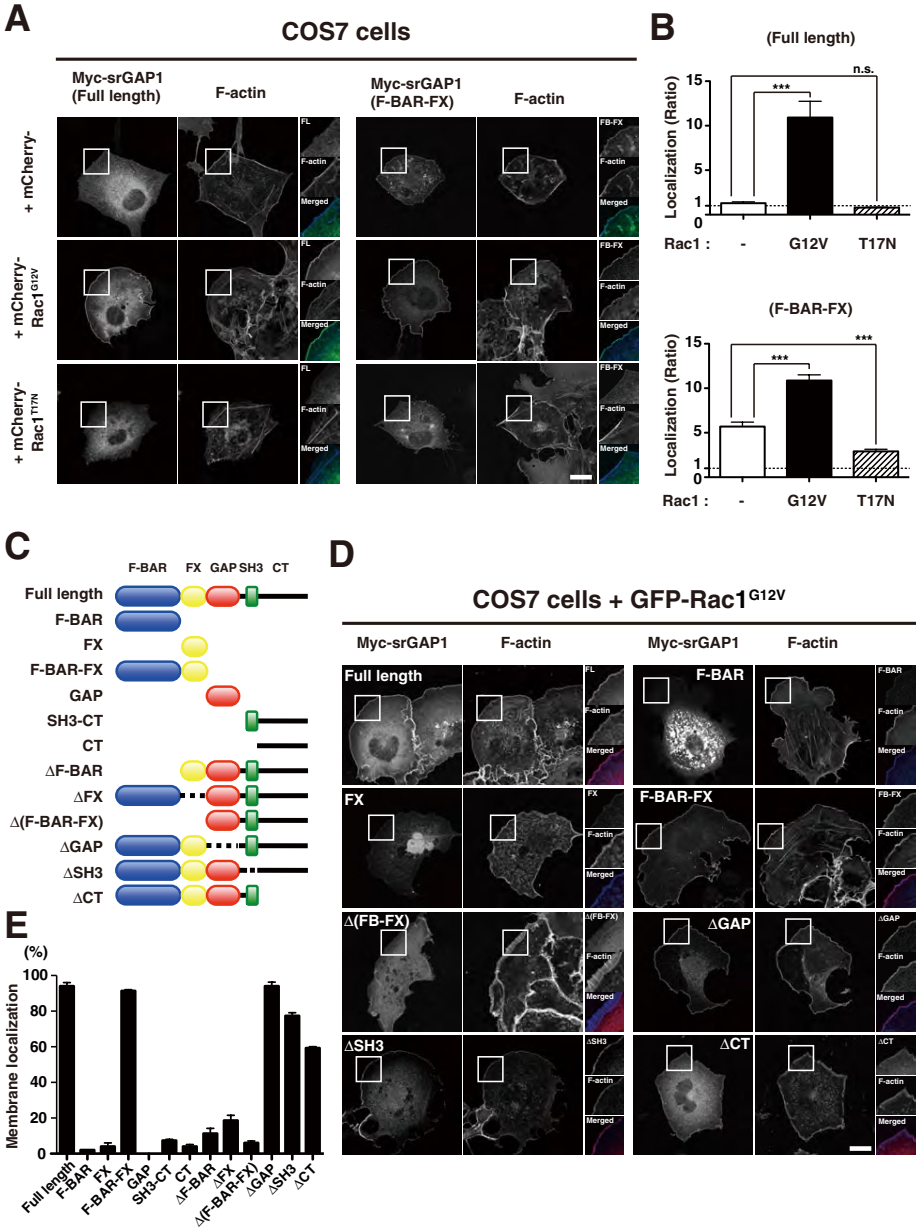

FIGURE 4: srGAP1 is recruited to the membrane protrusions through its F-BAR–FX unit, dependent on Rac1 signaling. (A) The effect of Rac1 signaling on the recruitment of srGAP1 to the membrane. Myc-srGAP1 (full length and F-BAR–FX) and mCherry-Rac1 (G12V and T17N) were coexpressed in COS7 cells. Cells were fixed and then stained for myc-srGAP1 (green) and F-actin (blue). The magnified images of the boxed areas are shown (top, myc; middle, F-actin; bottom, merged). Scale bar, 20 μm. (B) Quantification. The signal intensities of myc-srGAP1 (full length and F-BAR–FX) at the tip of the membrane protrusions were measured by ImageJ. The signal intensities at the tip of the membrane were normalized to those at the region 1 μm behind the tip. From three independent experiments, 45 protrusions of 15 cells were analyzed. Error bars indicate SEM. ***$p < 0.001$. (C) Constructs of srGAP1. (D) Myc-srGAP1 (full length, Δ(F-BAR-FX), F-BAR, FX, F-BAR–FX, ΔGAP, ΔSH3, and ΔCT) and GFP-Rac1^{G12V} were coexpressed in COS7 cells. Cells were fixed and then stained for myc-srGAP1 (green) and F-actin (blue). The magnified images of the boxed areas are shown. Scale bar, 20 μm. (E) Quantification. Cells in which myc-srGAP1 is localized at the tip of lamellipodial protrusions were counted. From three independent experiments, 150 cells were analyzed. Error bars, SEM.

F-BAR–FX unit and Rac1 interactions in Rac1-induced membrane localization of srGAP1. Because the CT region also bound with Rac1 (Figure 5B), such interaction might contribute Rac1-induced recruitment of srGAP1 to the membrane.

Rho/ROCK signaling regulates lamellipodial dynamics

How does srGAP1 regulate lamellipodial dynamics in a Rac1 activity–dependent manner? Rac1 is involved in the control of cell–substrate adhesion (Rottner *et al.*, 1999), and Rac1 depletion inhibited the development of the adhesive structures in HT1080 cells (Yamazaki *et al.*, 2009). Lamellipodia are stabilized by cell–substrate adhesion immediately behind their tips; defective adhesion causes their ruffling (Borm *et al.*, 2005; Giannone *et al.*, 2007). However, the adhesive structures were not observed behind the tips of spreading protrusions in srGAP1-depleted cells (Supplemental Figure S9).

Previous studies showed that RhoA is activated at the leading edge of the cell (Kurokawa and Matsuda, 2005; Pertz *et al.*, 2006; Machacek *et al.*, 2009), and our study demonstrated that RhoA and Rac1 activities increase toward lamellipodial protrusions in control cells (Figure 6A). In comparison, RhoA activation at lamellipodia was suppressed in srGAP1-depleted cells (Figure 6, A–D). As reported in previous studies (Kurokawa and Matsuda, 2005; Pertz *et al.*, 2006; Wu *et al.*, 2009), expression of Rac1^{G12V} repressed the activation of RhoA in a manner similar to srGAP1 depletion (Figure 6 E–G). Therefore the abolition of RhoA activity may underlie the abnormal lamellipodial dynamics caused by srGAP1 depletion. Indeed, expression of a constitutively active mutant of RhoA (RhoA^{G14V}) recovered membrane ruffling in srGAP1-depleted cells (Supplemental Figure S10).

RhoA regulates myosin II–based actomyosin contractility through ROCK-mediated phosphorylation of myosin regulatory light chain (MRLC; Narumiya *et al.*, 2009; Vicente-Manzanares *et al.*, 2009). Treatment with Y27632, a specific inhibitor of ROCK, decreased the phosphorylation level of MRLC at the cell periphery, including membrane protrusions (Supplemental Figure S11, A and B). In addition, constitutive activation of RhoA increased the amount of phosphorylated MRLC at the cell periphery in a manner dependent on ROCK in HT1080 cells (Supplemental Figure S11, A and B). Thus Rho/ROCK signaling mediates phosphorylation of MRLC at the cell periphery.

To define the importance of Rho/ROCK-induced actomyosin contractility, we examined lamellipodial dynamics in cells treated with blebbistatin, which is a specific inhibitor of myosin II, and Y27632. The treatment with blebbistatin and Y27632 decreased membrane ruffling and increased lamellipodial extent similarly to srGAP1 depletion (Supplemental Figures S12 and S13, control siRNA). Ectopic expression of the mutant ROCK

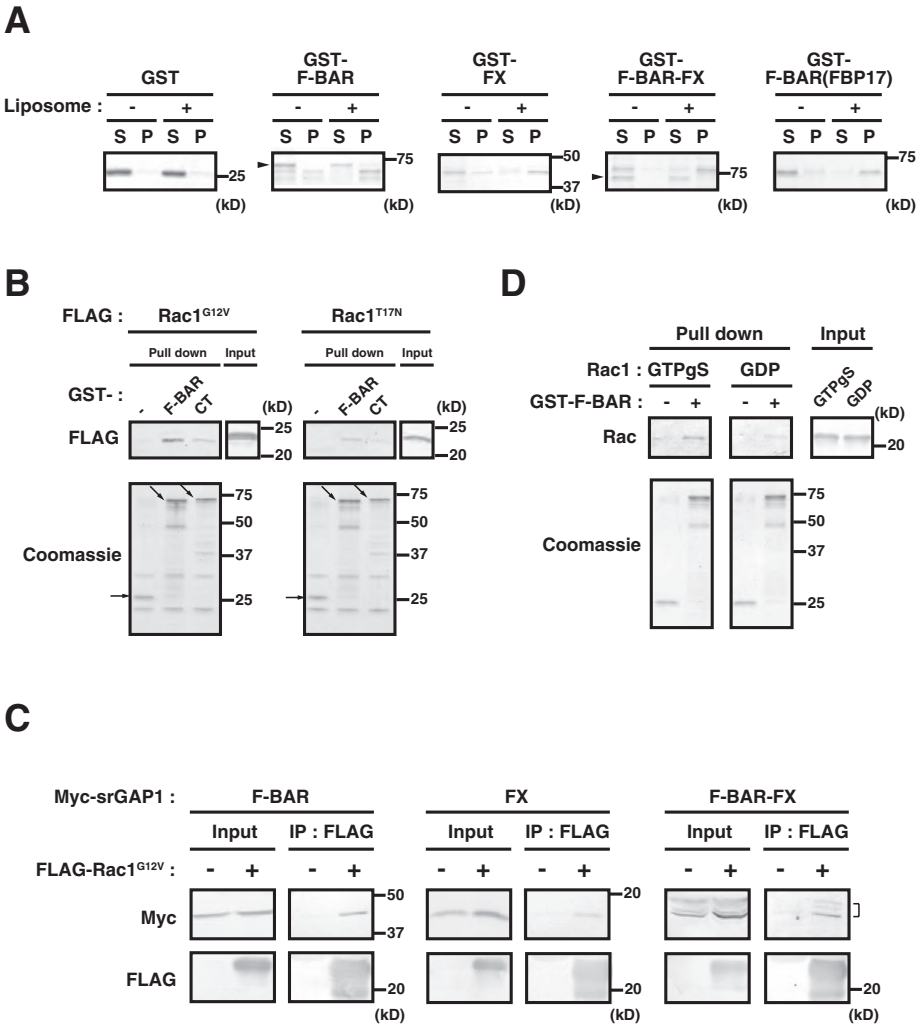

FIGURE 5: Characterization of the F-BAR–FX unit of srGAP1. (A) GST-fusion proteins were incubated with or without brain liposomes and then centrifuged. Supernatant (S) and pellet (P) were separated by SDS–PAGE. Proteins were detected by Coomassie brilliant blue. Arrowheads indicate a bacteria-derived protein copurified during affinity purification of GST-fusion proteins. (B) FLAG-Rac1^{G12V} and FLAG-Rac1^{T17N} were expressed in COS7 cells and then subjected to pull-down assay with GST-F-BAR and GST-CT, respectively. The bound proteins were analyzed by immunoblotting with anti-FLAG antibody. Arrows indicate GST-fusion proteins. (C) FLAG-Rac1^{G12V} and myc-srGAP1 (F-BAR, FX, and F-BAR–FX) were expressed in COS7 cells and then immunoprecipitated by anti-FLAG antibody. The bound proteins were analyzed by immunoblotting with anti- FLAG antibody. A bracket indicates FLAG-F-BAR–FX. (D) Bacterially expressed Rac1 was loaded with GTPγS (GTPgS) and GDP and subjected to pull-down assay with GST-F-BAR. The bound proteins were analyzed by immunoblotting with anti-Rac antibody.

protruding edge retracted toward the cell body (Figure 7A, arrows). These observations predict that the contractile force works not only perpendicular, but also parallel, to the extending edge. When the ruffling membrane stopped retracting, the next protruding membrane began to curl upward (Figure 7B, white broken lines). These observations suggest that the contractile force generated at the retracting membrane induces the next extending membrane to curl upward.

To examine whether depletion of srGAP1 affects actomyosin contractility, we performed time-lapse imaging of mCherry-tagged Lifeact, which is an indicator of actin (Riedl *et al.*, 2008), and VENUS-tagged MRLC in control and srGAP1-depleted cells. In control cells, actin filaments at the retracting membrane were gradually covered with myosin II, and a bundle-like structure was formed parallel to the edge of the extending protrusions (Figure 7C), as previously described (Svitkina *et al.*, 1997; Burnette *et al.*, 2011). The amount of Arp2/3 complex colocalized with the actin filaments gradually decreased as the actin filaments were covered with myosin II (Supplemental Figure S14A, compare red and green arrows). This result suggests that the actin filaments at the retracting membrane are converted from a branched structure containing the Arp2/3 complex to a bundled arrangement covered with myosin II (Supplemental Figure S14B). Indeed, it was reported that the mesh-like structure of actin filaments formed at the front of lamellipodia changed to a bundled one as the edge of lamellipodia retracted (Koestler *et al.*, 2008). Of importance, when actin filaments at the retracting membrane were covered with myosin II, the next extending membrane curled up (Figure 7C, arrows and arrowheads at 40 and 60 s).

In the srGAP1-depleted cells, myosin II showed a spot-like distribution, and colocalization of actin and myosin II was not observed at the spreading lamellipodia (Figure 7D). Although actin bundles were observed in lamellipodial protrusions, they were not covered with myosin II (Figure 7D, arrows and arrowheads). Thus the interaction between actin and myosin II and the formation of actomyosin bundles at the lamellipodia did not occur in srGAP1-depleted cells. The defective formation of actomyosin bundles at the base of the lamellipodia in srGAP1-depleted cells was recovered by reexpression of srGAP1 but not srGAP1^{R542A} (Figure 8, A and B). Furthermore, constitutive activation of Rac1 also inhibited actomyosin bundle formation, whereas loss of Rac1 promoted MRLC phosphorylation and development of cortical actomyosin bundles and membrane blebs dependent on ROCK (Figure 8B and Supplemental Figure S15). Of importance, treatment with blebbistatin or Y27632 also altered the distribution of myosin II and inhibited bundle formation at the lamellipodia (Figure 8B and Supplemental Figures S13, control siRNA,

(ROCKΔ3), which lacks a RhoA-binding site and acts as a dominant-active enzyme, increased the phosphorylated level of MRLC (Ishizaki *et al.*, 1997). In ROCKΔ3-expressing cells, phosphorylated MRLC left the cell periphery and concentrated in the center of the cell, and the lamellipodial morphology converted from ruffling to spreading (Supplemental Figure S11, C and D). These results suggest that Rho-mediated regulation of ROCK is important for control of lamellipodia. Thus Rho/ROCK signaling regulates lamellipodial dynamics through ROCK-induced myosin-based contractility.

Regulatory mechanism of membrane ruffling by actomyosin-based contractility

Analysis by phase-contrast microscopy demonstrated that the membrane began to curl upward from the lateral sides and then the

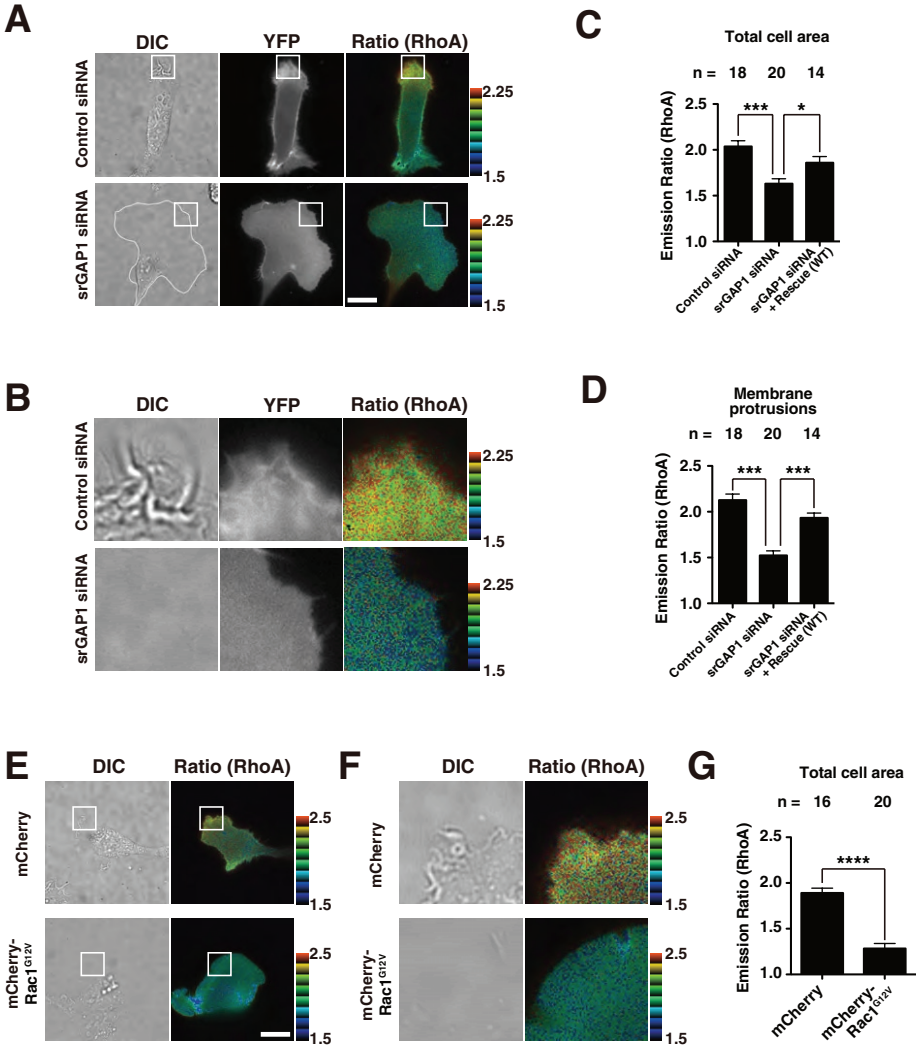

FIGURE 6: Imaging of RhoA activity. (A–D) Cells were treated with the indicated siRNAs and then transfected with FRET probes for RhoA. Cells were imaged for YFP, CFP, and DIC every 20 s for 20 min. FRET efficiencies are shown as YFP/CFP ratio images. White line indicates an outline of an srGAP1-depleted cell. (B) Magnified images of the boxed areas in A. Scale bar, 20 μm. (C, D) Emission ratio of YFP/CFP was measured at the entire region (C) and the membrane protrusions of the cells (D) by MetaMorph software. The total number of analyzed cells is shown above each bar. Three independent experiments were performed. Error bars, SEM. *$p < 0.05$, ***$p < 0.001$. (E–G) HT1080 cells were transfected with FRET probes for RhoA and the indicated expression vectors. Cells were imaged for YFP, CFP, and DIC every 20 s for 20 min. FRET efficiencies are shown as YFP/CFP ratio images. (F) The magnified images of the boxed areas in E. Scale bar, 20 μm. (G) Emission ratio of YFP/CFP measured at the membrane protrusions by MetaMorph software. The total number of analyzed cells is shown above each bar. Three independent experiments were performed. Error bars, SEM. Unpaired Student's *t* test indicates a significant difference between samples. ****$p < 0.0001$.

and S16). Collectively these results suggest that srGAP1 regulates Rho/ROCK signaling–mediated actomyosin contractility at lamellipodia via modulation of Rac1 activity.

srGAP1 regulates migratory behavior through lamellipodia formation

To examine the significance of srGAP1 in cell migration, we examined the relation between lamellipodial protrusions and migratory behavior by phase-contrast time-lapse microscopy in control and srGAP1-depleted cells. On collagen-coated substrate, the HT1080 cells showed random migration characterized by repeated directional changes (Figure 9A and Supplemental Movie S3). When a cell moved in a particular direction, only one compact lamellipodial protrusion was observed at the leading edge. The protrusion was then split into two or three, and the cells stopped moving (Figure 9A, arrows; Andrew and Insall, 2007). When all except one of the membrane protrusions were diminished, the cells began to move in the direction of the left protrusion. Thus cell movement correlates well with the dynamics of lamellipodial protrusions.

The lamellipodial protrusions spread larger and covered the majority of the cell periphery in srGAP1-depleted cells (Figure 9A); this severely inhibited cell locomotion (Figure 9A and Supplemental Movie S4). The frequency of the split of protrusions decreased and continuous protrusive structure was maintained in srGAP1-depleted cells (Figure 9B). To verify the effect of srGAP1 depletion on cell migration, we tracked cell movement and quantified their speed and directionality. Depletion of srGAP1 decreased migration velocity and increased rates of directional cell movement without affecting cell polarity (Figure 9, C–E, and Supplemental Figure S17). Reexpression of srGAP1, but not srGAP1^{R542A}, recovered the decreased velocity and increased the directionality of srGAP1-depleted cells. Thus srGAP1 depletion altered the dynamics of protrusions and changed the cell migratory mode from random to directionally persistent.

DISCUSSION

Overactivation of Rac1 causes development of continuous lamellipodial protrusions around the cell, whereas suppression of Rac1 activity inhibits their formation (Pankov *et al.*, 2005). Cell migration is severely repressed in both cases, and thus spatiotemporal activation of Rac1 must be tightly regulated. However, it remains unknown how the level of Rac activity is modulated at lamellipodial protrusions. In this study, we showed that srGAP1 inhibits excessive increase in Rac1 activity at lamellipodia via its RacGAP activity (Figure 10A). srGAP1 is recruited to the lamellipodia in a Rac1-dependent manner, and therefore Rac1 and srGAP1 constitute a negative feedback loop that can limit the maximum intensity of Rac1 signaling (Brandman and Meyer, 2008). Depletion of srGAP1 spatially propagates Rac1 activity throughout the cells, and the structure of cell–substrate adhesions at the lamellipodia is larger in srGAP1-depleted than control cells (Supplemental Figure S9). The positive feedback between increased cell–substrate adhesion and Rac1 activation (Nayal *et al.*, 2006) implies that development of adhesive structures might induce propagation of activated Rac1 throughout the cell in srGAP1-depleted cells.

Here we show that srGAP1 controls membrane ruffling through the coordination of Rac1 and RhoA. Rac1 induces actin

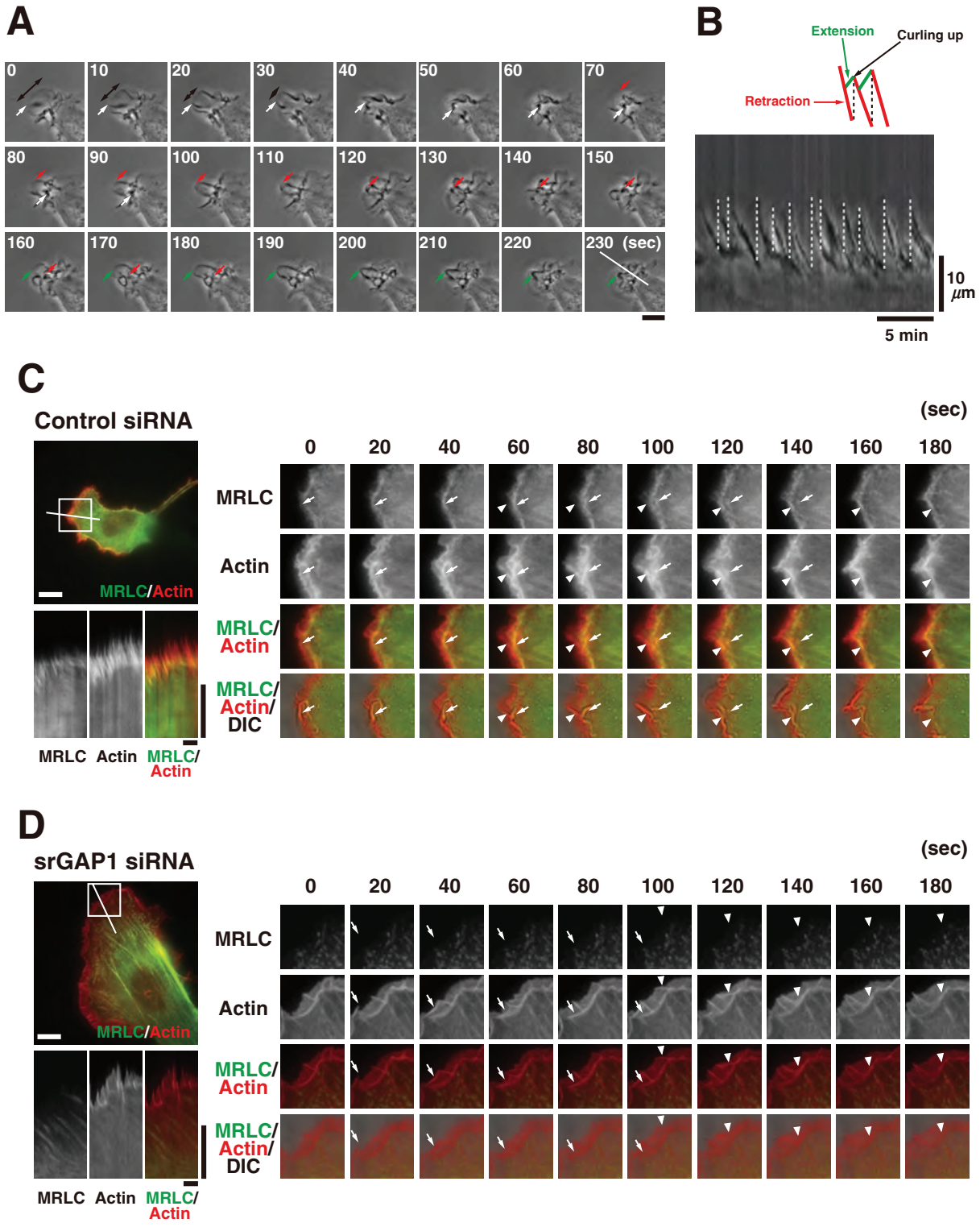

FIGURE 7: Myosin-based contractility causes membrane ruffling. (A) Time-lapse montage of the ruffling membranes. HT1080 cells were plated on collagen-coated, glass-bottomed dishes. Membrane dynamics were observed by phase-contrast microscopy. White, red, and green arrows indicate the edges of distinct membrane protrusions. Black double-headed arrows indicate a change in extent of membrane protrusion. The kymograph shown in B was generated along the white line. Scale bar, 10 μm. (B) Kymograph analysis. White broken lines indicate the timing of ruffling of the membrane protrusions. Scale bars, 10 μm (vertical), 5 min (horizontal). (C, D) Myosin II dynamics. HT1080 cells were treated with control (C) or srGAP1 RNAi (D) and then transfected with VENUS-MRLC (green) and Lifeact-mCherry (red). Kymographs were generated along the white line. Time-lapse images of the area indicated by the white square are shown. Scale bars, 10 μm (white), 10 μm (vertical, kymograph), and 5 min (horizontal, kymograph). Arrows and arrowheads in C indicate the retracting edge of the membrane protrusions. Arrows and arrowheads in D and E indicate actin bundles crossing through lamellipodia.

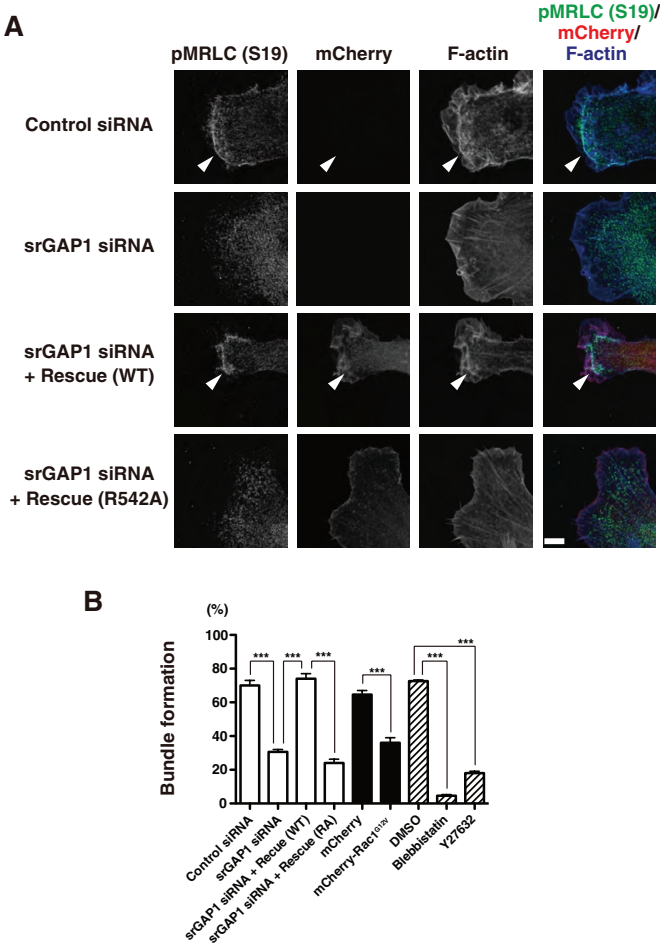

FIGURE 8: Actomyosin contractile bundles at lamellipodia. (A) HT1080 cells transfected with the indicated siRNAs and the mCherry-tagged rescue constructs (red) were stained for phosphorylated MRLC (S19) (green) and F-actin (blue). Arrowheads indicate the actomyosin contractile bundles. Scale bar, 10 μm. (B) Quantification. Cells with actomyosin bundles at the base of the sheet-like membrane protrusions were counted. One hundred fifty cells were analyzed from three independent experiments. Error bars, SEM. ***$p < 0.001$.

reorganization that is essential for membrane extension at the tip of lamellipodial protrusions. Therefore it is possible that membrane protrusion is terminated by srGAP1-dependent inactivation of Rac1, which is followed by membrane retraction in response to decreased Rac1 activity. However, no significant decrease in Rac1 activity was detected in the retracting phase of ruffling membranes (Supplemental Figure S4). Moreover, in previous studies, retraction of lamellipodia did not necessarily accompany decrease in Rac1 activity (Kurokawa *et al.*, 2004; Machacek *et al.*, 2009). Therefore we conclude that the contribution of srGAP1 to membrane ruffling does not occur through temporal inactivation of Rac1 at lamellipodia during one protrusion–retraction cycle.

On the basis of these results, we propose a model of srGAP1-mediated control of lamellipodial dynamics (Figure 10B). We propose that activated Rac1 induces membrane protrusions by promoting actin polymerization via the Arp2/3 complex, and, subsequently, that srGAP1 is recruited to the membrane in a manner dependent on Rac1 activity and represses excessive activation of Rac1. This spatially restricts the propagation of membrane protrusions and enables the concomitant activation of Rac1 and RhoA at the lamellipodia. RhoA activates ROCK and stimulates actomyosin contractility, causing periodic membrane ruffling. Such compact, dynamic, ruffling protrusions often bifurcate and cause frequent directional changes during cell migration, leading to random motility. Thus srGAP1 is a key determinant of lamellipodial dynamics and intrinsic cell migratory behavior.

Cells have the ability to spontaneously generate cell polarity with lamellipodia at their leading edges. This polarity is heavily influenced by chemoattractants, which direct cells by biasing the intrinsic lamellipodial dynamics toward the source (Petrie *et al.*, 2009). It has been suggested that positive feedback signaling via PIP_3 (phosphatidylinositol (3,4,5)-triphosphate) or other molecules contributes to polarity establishment during cell migration through the generation of lamellipodia. In this study, we demonstrate that srGAP1-mediated negative feedback regulation of Rac signaling dictates the dynamic behavior of lamellipodia and spatially restricts the propagation of lamellipodia, producing compact lamellipodial protrusions. Thus the balance between positive and negative feedback signaling is crucial for normal lamellipodial dynamics. This is a new concept on the control of lamellipodia in motile cells.

MATERIALS AND METHODS

Cell culture

The HT1080 human fibrosarcoma cells and COS7 cells were cultured in DMEM (Wako, Osaka, Japan) supplemented with 10% fetal bovine serum (FBS). FreeStyle 293-F cells were cultured in FreeStyle 293 Expression medium (Invitrogen, Carlsbad, CA). HT1080 cells were plated on glass-bottomed dishes and coverslips (Mastunami, Osaka, Japan) coated with type I collagen (0.3 mg/mL; Nitta Gelatin, Osaka, Japan) at room temperature for 30 min.

Plasmids

Full-length human *srGAP1* and *srGAP2* cDNAs were purchased from Open Biosystems. Full-length human *MRLC* (*MYL12B*), *RhoA*, *Rac1*, and *Cdc42* cDNAs were obtained by PCR using human whole brain cDNA (Clontech, Mountain View, CA). Site-directed mutagenesis was performed using the PrimeSTAR MAX DNA polymerase according to the manufacturer's instructions (TaKaRa Bio, Otsu, Japan). Site-directed mutagenesis was used to mutate Arg-542 and Trp-780 of srGAP1 to alanine, Gly-14 of RhoA and Gly-12 of Rac1 and Cdc42 to valine, and Thr-17 of Rac1 to asparagine. The following deletion mutants of srGAP1 were amplified by PCR: F-BAR (amino acids [aa] 1–363), FX (aa 364–503), F-BAR–FX (aa 1–503), GAP (aa 504–687), SH3-CT (aa 743–1085), SH3 (aa 743–802), CT (aa 803–1085), ΔF-BAR (aa 364–1085), and ΔF-BAR–FX (aa 504–1085). The following deletion mutants of srGAP1 were generated by site-directed mutagenesis: ΔFX (aa 1–363 + 504–1085), ΔGAP (aa 1–503 + 688–1085), ΔSH3 (aa 1–742 + 803–1085), and ΔCT (aa 1–802). All cDNAs were sequenced and then cloned into the pEF-BOS vector (Mizushima and Nagata, 1990) encoding an N-terminal FLAG tag or myc tag, pEGFP-C1, pEGFP-N3, pmCherry-C1 (Clontech), and pGEX-6P-1 (GE Healthcare, Piscataway, NJ). To create the VENUS-fusion constructs, *GFP* genes in the green fluorescent protein (GFP) fusion constructs were replaced by the *VENUS* gene (Nagai *et al.*, 2002). The glutathione *S*-transferase (GST)–FBP17, GFP-F-BAR–FX (Fer), and GFP-IRSp53 constructs have been previously described (Suetsugu *et al.*, 2006; Tsujita *et al.*, 2006; Itoh *et al.*, 2009). The myc-tagged ROCKΔ3 construct was provided by Y. Takai (Kobe University, Kobe, Japan).

Transfection

The plasmids were transfected into HT1080 cells by using FuGENE HD Transfection reagent, according to the manufacturer's manual

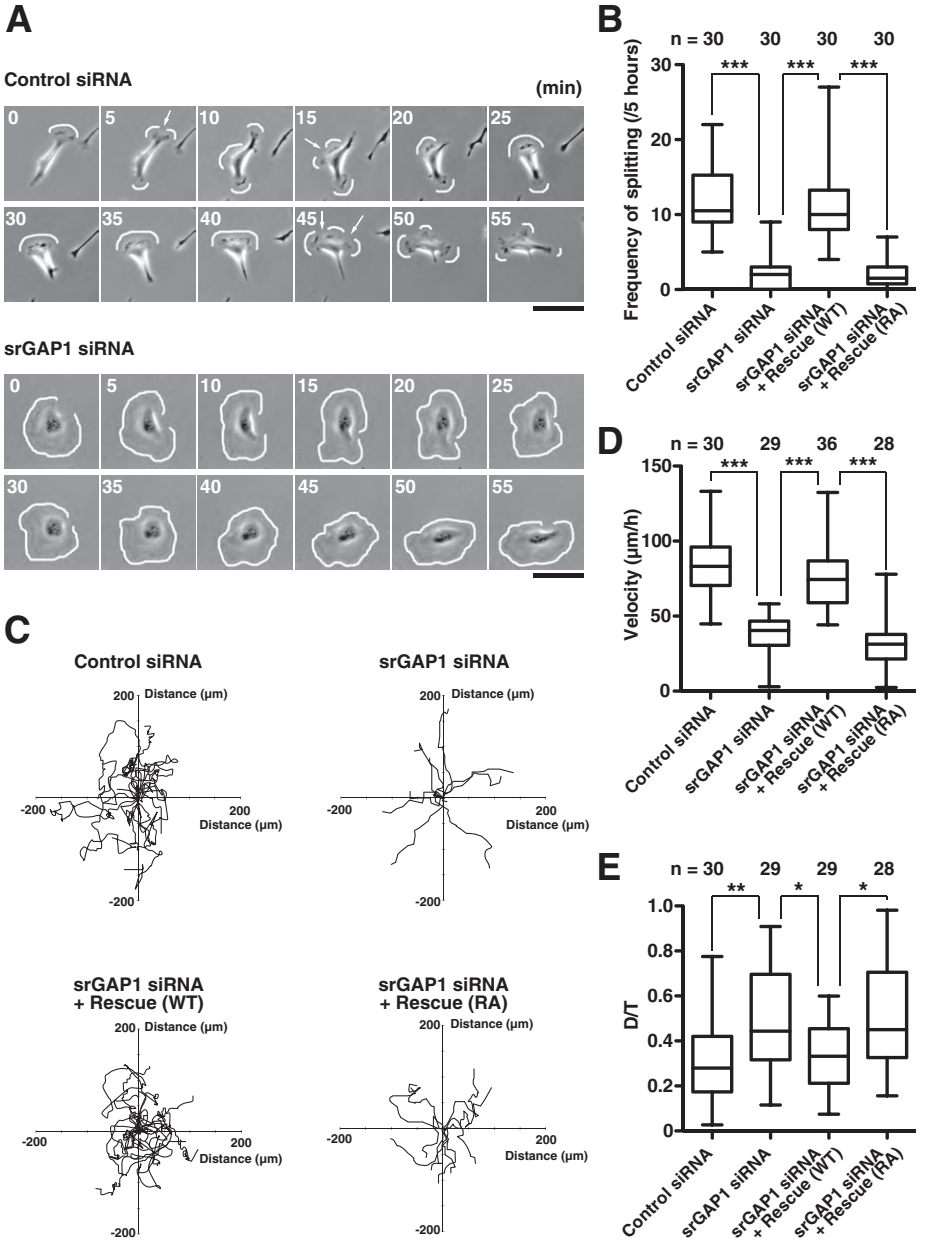

FIGURE 9: srGAP1 regulates the cellular migratory behavior. (A) Morphological changes of the motile cells. HT1080 cells treated with control or srGAP1-directed siRNA were plated on collagen-coated, glass-bottomed dishes, and cell migration was monitored by phase-contrast microscopy. White curves indicate the position of the sheet-like membrane protrusions. Arrows indicate the splitting of the protrusions. Scale bar, 100 μm. (B) Quantification of the frequency of splitting of the protrusions. The number of splittings of the membrane protrusions in each cell for 5 h were counted. Three independent experiments were performed. The total number of analyzed cells is shown above each bar. Error bars, SEM. ***$p < 0.001$. (C) Migration tracks of cells plated on collagen-coated substrates. Ten cells from three independent experiments. (D) Quantification of migratory velocity. The total number of analyzed cells is shown above each bar. Three independent experiments were performed. ***$p < 0.001$. (E) Quantification of the persistence of migratory directionality. D/T is the ratio of the direct distance (D) divided by the total track distance (T). The total number of analyzed cells is shown above each bar. Three independent experiments were performed. Error bars, SEM. *$p < 0.05$, **$p < 0.01$.

(Roche, Indianapolis, IN). The plasmids were transfected into COS7 cells by using Lipofectamine LTX reagent, according to the manufacturer's manual (Invitrogen). The plasmids were transfected into FreeStyle 293F cells with FreeStyle MAX reagent according to the manufacturer's instructions (Invitrogen).

RNAi

The cells were cultured for 48–72 h after the stealth siRNAs (Invitrogen) were transfected into the HT1080 cells with Lipofectamine RNAiMAX reagent (Invitrogen). The target sequences were as follows: srGAP1 siRNA#1, 5′-CCAGUCCAGGCAGAGCUCAUGCUCA-3′; srGAP1 siRNA#2, 5′-GGUGCAGGAUAUGGAUGAUACGUUU-3′; srGAP1 siRNA#3, 5′-CACCCAGAAUGGGCGUGCAGCUGAA-3′. siRNA#1 was used to deplete srGAP1, unless noted otherwise. The target sequences of the control siRNA and Rac1 siRNA have been previously described (Yamazaki *et al.*, 2009). The rescue constructs (srGAP1 siRNA#1 resistant and base pair mutations A1059T, G1062A, C1063T, and C1065G) were generated with site-directed mutagenesis as described. The rescue constructs were introduced 24 h after transfection of srGAP1 siRNA#1.

Reagents

The anti-srGAP1 antibody (sc-81939) and anti-RhoA antibody (sc-418) were purchased from Santa Cruz, Santa Cruz, CA. The anti-Myc (2272) and anti-phospho-myosin Light Chain 2 (Ser-19) antibodies (3671) were purchased from Cell Signaling Technology, Danvers, MA. The anti-FLAG (F3165) and anti-vinculin antibodies (V9131) were purchased from Sigma-Aldrich, St. Louis, MO. The anti-p34 (07-227) and anti-Rac1 antibodies (05-389) were purchased from Upstate, Billerica, MA. The anti-Cdc42 (610928), anti-GM130 (610822), and anti-paxillin antibodies (610051) were purchased from BD Biosciences, San Jose, CA. The anti-actin antibody (MAB1501) was purchased from Millipore, Billerica, MA. Rhodamine-labeled phalloidin and Alexa Fluor 647–labeled phalloidin were purchased from Molecular Probes, Eugene, OR. Blebbistatin and Y-27632 were purchased from Calbiochem, Temecula, CA.

Immunofluorescence and microscopy

The cells were plated on coverslips and then fixed with 4% paraformaldehyde for 10 min at room temperature, following permeabilization using 0.2% Triton X-100 in phosphate-buffered saline (PBS) for 5 min. Before staining for paxillin and vinculin, the cells were fixed with PBS containing 2% paraformaldehyde and 0.05% Triton X-100 for 2 min on ice. The coverslips were washed twice with PBS and fixed with 4% paraformaldehyde for 5 min on ice. The coverslips were incubated with the primary antibodies for 1 h at room temperature or 12 h at 4°C and then with the secondary antibodies for 30 min at room temperature. The coverslips were mounted with PermaFluor Aqueous Mounting Medium (Thermo Scientific,

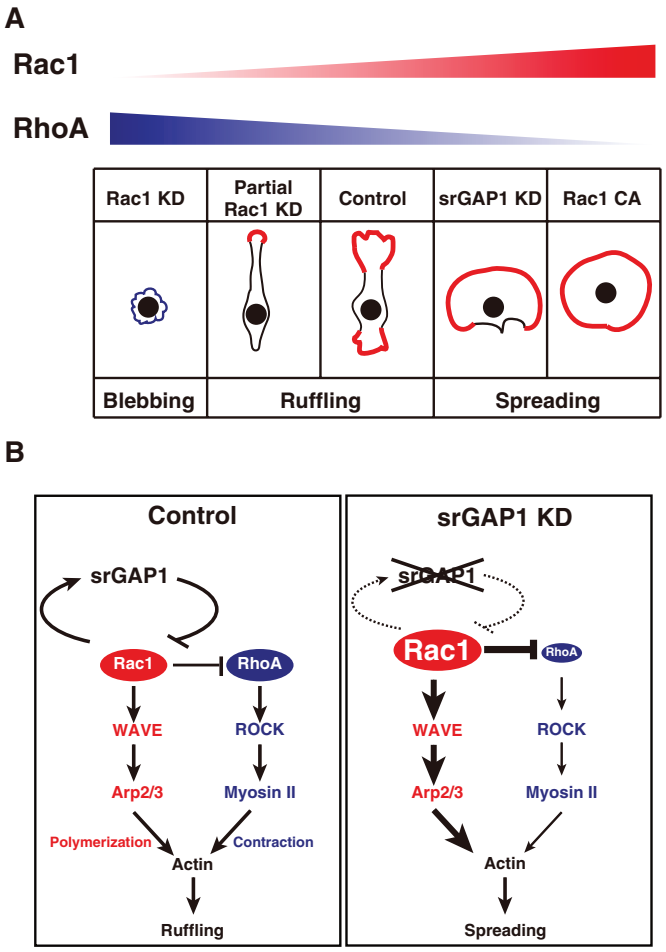

FIGURE 10: Summary. (A) The level of Rac1 activity controls the membrane protrusions. (B) Limitation of Rac1 activity by srGAP1 allows concomitant activation of Rac1 and RhoA at the membrane protrusions.

Waltham, MA) and observed using a FluoView 1000-D confocal microscope (Olympus, Tokyo, Japan).

Kymographic analysis

For kymography, phase-contrast time-lapse sequences were obtained using IP Lab software and the 40× objective. The video clips were 20 min long, with images captured every 20 s. The kymographs were produced and analyzed using the ImageJ software (National Institutes of Health, Bethesda, MD).

FRET

The FRET probes for Rac1 and RhoA, Raichu-Rac and Raichu-RhoA, respectively, have been previously described (Itoh *et al.*, 2002; Kurokawa and Matsuda, 2005). The HT1080 cells were transfected with FRET probes and plated onto collagen-coated, glass-bottomed dishes (Matsunami). During time-lapse imaging, the cells were cultured in medium containing 10 mM 4-(2-hydroxyethyl)-1-piperazineethanesulfonic acid (HEPES; pH 7.5), 150 mM NaCl, 5 mM KCl, 1 mM $CaCl_2$, 1 mM $MgCl_2$, and 10 mM glucose supplemented with 10% FBS. The cells were imaged using an Olympus IX81 inverted microscope equipped with a charge-coupled device camera (Cascade II 512; Photometrics) controlled by MetaMorph software (Universal Imaging, Bedford Hills, NY). The cells were illuminated with a xenon lamp through a 6% ND filter (Olympus) and a 100× oil immersion objective lens. The images were collected at 20-s intervals for 20 min. After background subtraction, the ratio image of yellow fluorescent protein (YFP)/cyan fluorescent protein (CFP) was determined using MetaMorph and the ratio used to represent FRET efficiency.

Time-lapse imaging

Time-lapse imaging of VENUS-MRLC and mCherry-Lifeact in the HT1080 cells was performed as described for FRET. Time-lapse images of VENUS-MRLC and mCherry-Lifeact were collected at 20-s intervals for 20 min. Time-lapse imaging of the F-BAR–FX unit of srGAP1 and srGAP2 in the COS7 cells was performed using a FluoView 1000-D confocal microscope. The time-lapse images were collected at 10-s intervals for 10 min.

Migration assay

Time-lapse microscopic observations of cell motility were performed using cells plated onto collagen-coated, 35-mm glass-bottomed dishes. After 1 h, the cells were observed for >5 h by using an Axiovert S100 system and a 10× objective lens (Carl Zeiss, Jena, Germany). The images were collected at 5-min intervals, and the velocity and persistence of the migratory directionality were determined by tracking the positions of cell nuclei with ImageJ software. The *D*/*T* ratios indicate the direct distance from the start to end point (*D*) divided by the total track distance (*T*), as previously described (Pankov *et al.*, 2005).

Protein purification

Human full-length *srGAP1* was cloned into the pEF-BOS vector encoding an N-terminal FLAG tag and transfected into FreeStyle 293-F cells. The cells were harvested by centrifugation 72 h after transfection, and the pellet was resuspended in lysis buffer (40 mM Tris, pH 7.5, 150 mM NaCl, and 0.5% Triton X-100) supplemented with Complete EDTA-free Protease Inhibitor Cocktail Tablet (Roche). The cells were lysed by sonication and centrifuged at 20,000 × *g* for 10 min. The anti-FLAG M2 affinity gel (Sigma-Aldrich) was incubated with the supernatant for 2 h and then washed with lysis buffer. FLAG-srGAP1 was eluted with the competing 3× FLAG peptide (Sigma-Aldrich). Human full-length *Rac1* and the F-BAR, FX, F-BAR–FX domains of human *srGAP1* were cloned into the pGEX-6P-1 vector (GE Healthcare). These constructs were used to transform BL21 (DE3) pLysS *Escherichia coli* (Promega, Madison, WI) cells. The cells expressing the GST-fusion proteins were collected and resuspended in lysis buffer, lysed by sonication, and centrifuged at 20,000 × *g* for 10 min. Glutathione Sepharose 4B was incubated with the supernatant for 2 h and then washed with lysis buffer. GST was cleaved from GST-Rac1 with PreScission Protease (GE Healthcare). For the cosedimentation assay, GST-F-BAR, GST-FX, and GST-F-BAR–FX were eluted with elution buffer (50 mM Tris, pH 7.5, 50 mM glutathione).

Effecter pull-down assays

The amounts of active RhoA, Rac1, and Cdc42 were investigated in pull-down assays with GST-Rhotekin-RBD (RhoA) and GST-PAK-CRIB (Rac1 and Cdc42) as previously described (Yamazaki *et al.*, 2009). The signal intensities were measured using ImageJ.

In vitro GAP assay

The bacterially expressed Rac1 described earlier was loaded with GTP into loading buffer (50 mM Tris, pH 7.5, 5 mM EDTA, 50 μM GTP, and 0.4 μM Rac1). Loading was performed for 10 min at 30°C, followed by addition of 20 mM $MgCl_2$ and further incubation for

10 min on ice. GTP-loaded Rac1 was incubated with or without FLAG-srGAP1 in GAP buffer (20 mM Tris, pH 7.5, 0.1 mM dithiothreitol, 0.86 mg/ml BSA, 40 nM Rac1, and 6 nM FLAG-srGAP1) for 10 min at 30°C, followed by addition of 5 mM $MgCl_2$. The amount of GTP-bound Rac1 was measured by pull-down assay with GST-PAK-CRIB.

Liposome cosedimentation assay

Liposomes (1 mg/ml) and GST fusion proteins (10 μg/ml) were incubated in buffer containing 20 mM HEPES, pH 7.4, 100 mM NaCl, and 2 mM EDTA. The mixtures were collected by centrifugation at 100,000 × *g* for 30 min. The supernatants and pellets were analyzed by SDS–PAGE and Coomassie staining.

Immunoprecipitation

The COS7 cells transfected with the FLAG tag constructs were cultured for 24 h and then collected with lysis buffer supplemented with the Protease Inhibitor Cocktail. The cells were lysed by sonication and centrifuged at 20,000 × *g* for 10 min. The anti-FLAG M2 affinity gel was incubated with the supernatant for 2 h and then washed thrice with lysis buffer and incubated with SDS-sample buffer.

Pull-down assay

The HT1080 and COS7 cells were collected and added to lysis buffer supplemented with the Protease Inhibitor Cocktail. The cells were lysed by sonication and centrifuged at 20,000 × *g* for 10 min. Glutathione Sepharose 4B bound to GST-fusion proteins was incubated with cell lysates or purified proteins for 2 h and then washed thrice with lysis buffer and incubated with SDS-sample buffer.

Statistical analysis

Statistical analysis was performed using Prism 5 (Graphpad, La Jolla, CA). Tukey's multiple comparison test was used after one-way analysis of variance to calculate *p* values. In Figure 1, E and G, and Supplemental Figure S12B, Dunn's multiple comparison test was used after the Kruskal–Wallis test to calculate *p* values.

ACKNOWLEDGMENTS

We thank Michiyuki Matsuda for providing FRET probes, Yoshimi Takai for providing the ROCK I construct, and Takenawa and Itoh lab members for helpful comments and discussions.

REFERENCES

Andrew N, Insall RH (2007). Chemotaxis in shallow gradients is mediated independently of PtdIns 3-kinase by biased choices between random protrusions. Nat Cell Biol 9, 193–200.

Borm B, Requardt RP, Herzog V, Kirfel G (2005). Membrane ruffles in cell migration: indicators of inefficient lamellipodia adhesion and compartments of actin filament reorganization. Exp Cell Res 302, 83–95.

Bos JL, Rehmann H, Wittinghofer A (2007). GEFs and GAPs: critical elements in the control of small G proteins. Cell 129, 865–877.

Brandman O, Meyer T (2008). Feedback loops shape cellular signals in space and time. Science 322, 390–395.

Burnette DT, Manley S, Sengupta P, Sougrat R, Davidson MW, Kachar B, Lippincott-Schwartz J (2011). A role for actin arcs in the leading-edge advance of migrating cells. Nat Cell Biol 13, 371–381.

Burridge K, Wennerberg K (2004). Rho and Rac take center stage. Cell 116, 167–179.

Carlson BR, Lloyd KE, Kruszewski A, Kim IH, Rodriguiz RM, Heindel C, Faytell M, Dudek SM, Wetsel WC, Soderling SH (2011). WRP/srGAP3 facilitates the initiation of spine development by an inverse F-BAR domain, and its loss impairs long-term memory. J Neurosci 31, 2447–2460.

Coutinho-Budd J, Ghukasyan V, Zylka MJ, Polleux F (2012). The F-BAR domains from srGAP1, srGAP2 and srGAP3 regulate membrane deformation differently. J Cell Sci 125, 3390–3401.

de Kreuk BJ, Nethe M, Fernandez-Borja M, Anthony EC, Hensbergen PJ, Deelder AM, Plomann M, Hordijk PL (2011). The F-BAR domain protein PACSIN2 associates with Rac1 and regulates cell spreading and migration. J Cell Sci 124, 2375–2388.

Endris V, Haussmann L, Buss E, Bacon C, Bartsch D, Rappold G (2011). SrGAP3 interacts with lamellipodin at the cell membrane and regulates Rac-dependent cellular protrusions. J Cell Sci 124, 3941–3955.

Foletta VC, Brown FD, Young WS 3rd (2002). Cloning of rat ARHGAP4/C1, a RhoGAP family member expressed in the nervous system that colocalizes with the Golgi complex and microtubules. Brain Res Mol Brain Res 107, 65–79.

Giannone G *et al*. (2007). Lamellipodial actin mechanically links myosin activity with adhesion-site formation. Cell 128, 561–575.

Guerrier S, Coutinho-Budd J, Sassa T, Gresset A, Jordan NV, Chen K, Jin WL, Frost A, Polleux F (2009). The F-BAR domain of srGAP2 induces membrane protrusions required for neuronal migration and morphogenesis. Cell 138, 990–1004.

Guo S, Bao S (2010). srGAP2 arginine methylation regulates cell migration and cell spreading through promoting dimerization. J Biol Chem 285, 35133–35141.

Habermann B (2004). The BAR-domain family of proteins: a case of bending and binding? EMBO Rep 5, 250–255.

Ishizaki T, Naito M, Fujisawa K, Maekawa M, Watanabe N, Saito Y, Narumiya S (1997). p160ROCK, a Rho-associated coiled-coil forming protein kinase, works downstream of Rho and induces focal adhesions. FEBS Lett 404, 118–124.

Itoh T, Erdmann KS, Roux A, Habermann B, Werner H, De Camilli P (2005). Dynamin and the actin cytoskeleton cooperatively regulate plasma membrane invagination by BAR and F-BAR proteins. Dev Cell 9, 791–804.

Itoh T, Hasegawa J, Tsujita K, Kanaho Y, Takenawa T (2009). The tyrosine kinase Fer is a downstream target of the PLD-PA pathway that regulates cell migration. Sci Signal 2, ra52.

Itoh RE, Kurokawa K, Ohba Y, Yoshizaki H, Mochizuki N, Matsuda M (2002). Activation of rac and cdc42 video imaged by fluorescent resonance energy transfer-based single-molecule probes in the membrane of living cells. Mol Cell Biol 22, 6582–6591.

Koestler SA, Auinger S, Vinzenz M, Rottner K, Small JV (2008). Differentially oriented populations of actin filaments generated in lamellipodia collaborate in pushing and pausing at the cell front. Nat Cell Biol 10, 306–313.

Kurokawa K, Itoh RE, Yoshizaki H, Nakamura YO, Matsuda M (2004). Coactivation of Rac1 and Cdc42 at lamellipodia and membrane ruffles induced by epidermal growth factor. Mol Biol Cell 15, 1003–1010.

Kurokawa K, Matsuda M (2005). Localized RhoA activation as a requirement for the induction of membrane ruffling. Mol Biol Cell 16, 4294–4303.

Machacek M, Hodgson L, Welch C, Elliott H, Pertz O, Nalbant P, Abell A, Johnson GL, Hahn KM, Danuser G (2009). Coordination of Rho GTPase activities during cell protrusion. Nature 461, 99–103.

Malliri A, Collard JG (2003). Role of Rho-family proteins in cell adhesion and cancer. Curr Opin Cell Biol 15, 583–589.

Mason FM, Heimsath EG, Higgs HN, Soderling SH (2011). Bi-modal regulation of a formin by srGAP2. J Biol Chem 286, 6577–6586.

Miki H, Yamaguchi H, Suetsugu S, Takenawa T (2000). IRSp53 is an essential intermediate between Rac and WAVE in the regulation of membrane ruffling. Nature 408, 732–735.

Mizushima S, Nagata S (1990). pEF-BOS, a powerful mammalian expression vector. Nucleic Acids Res 18, 5322.

Nagai T, Ibata K, Park ES, Kubota M, Mikoshiba K, Miyawaki A (2002). A variant of yellow fluorescent protein with fast and efficient maturation for cell-biological applications. Nat Biotechnol 20, 87–90.

Narumiya S, Tanji M, Ishizaki T (2009). Rho signaling ROCK and mDia1, in transformation, metastasis and invasion. Cancer Metastasis Rev 28, 65–76.

Nayal A, Webb DJ, Brown CM, Schaefer EM, Vicente-Manzanares M, Horwitz AR (2006). Paxillin phosphorylation at Ser273 localizes a GIT1-PIX-PAK complex and regulates. adhesion and protrusion dynamics. J Cell Biol 173, 587–589.

Neukomm LJ *et al*. (2011). Loss of the RhoGAP SRGP-1 promotes the clearance of dead and injured cells in *Caenorhabditis elegans*. Nat Cell Biol 13, 79–86.

Pankov R, Endo Y, Even-Ram S, Araki M, Clark K, Cukierman E, Matsumoto K, Yamada KM (2005). A Rac switch regulates random versus directionally persistent cell migration. J Cell Biol 170, 793–802.

Pertz O (2010). Spatio-temporal Rho GTPase signaling—where are we now? J Cell Sci 123, 1841–1850.

Pertz O, Hodgson L, Klemke RL, Hahn KM (2006). Spatiotemporal dynamics of RhoA activity in migrating cells. Nature 440, 1069–1072.
Petrie RJ, Doyle AD, Yamada KM (2009). Random versus directionally persistent cell migration. Nat Rev Mol Cell Biol 10, 538–549.
Pollard TD, Borisy GG (2003). Cellular motility driven by assembly and disassembly of actin filaments. Cell 112, 453–465.
Ridley AJ (2011). Life at the leading edge. Cell 145, 1012–1022.
Ridley AJ, Schwartz MA, Burridge K, Firtel RA, Ginsberg MH, Borisy G, Parsons JT, Horwitz AR (2003). Cell migration: integrating signals from front to back. Science 302, 1704–1709.
Riedl J *et al*. (2008). Lifeact: a versatile marker to visualize F-actin. Nat Methods 5, 605–607.
Rottner K, Hall A, Small JV (1999). Interplay between Rac and Rho in the control of substrate contact dynamics. Curr Biol 9, 640–648.
Sarmiento C *et al*. (2008). WASP family members and formin proteins coordinate regulation of cell protrusions in carcinoma cells. J Cell Biol 180, 1245–1260.
Small JV, Resch GP (2005). The comings and goings of actin: coupling protrusion and retraction in cell motility. Curr Opin Cell Biol 17, 517–523.
Soderling SH, Binns KL, Wayman GA, Davee SM, Ong SH, Pawson T, Scott JD (2002). The WRP component of the WAVE-1 complex attenuates Rac-mediated signalling. Nat Cell Biol 4, 970–975.
Suetsugu S, Murayama K, Sakamoto A, Hanawa-Suetsugu K, Seto A, Oikawa T, Mishima C, Shirouzu M, Takenawa T, Yokoyama S (2006). The RAC binding domain/IRSp53-MIM homology domain of IRSp53 induces RAC-dependent membrane deformation. J Biol Chem 281, 35347–35358.
Svitkina TM, Verkhovsky AB, McQuade KM, Borisy GG (1997). Analysis of the actin-myosin II system in fish epidermal keratocytes: mechanism of cell body translocation. J Cell Biol 139, 397–415.
Takenawa T, Suetsugu S (2007). The WASP-WAVE protein network: connecting the membrane to the cytoskeleton. Nat Rev Mol Cell Biol 8, 37–48.
Tcherkezian J, Lamarche-Vane N (2007). Current knowledge of the large RhoGAP family of proteins. Biol Cell 99, 67–86.
Tsujita K, Suetsugu S, Sasaki N, Furutani M, Oikawa T, Takenawa T (2006). Coordination between the actin cytoskeleton and membrane deformation by a novel membrane tubulation domain of PCH proteins is involved in endocytosis. J Cell Biol 172, 269–279.
Vicente-Manzanares M, Ma X, Adelstein RS, Horwitz AR (2009). Non-muscle myosin II takes centre stage in cell adhesion and migration. Nat Rev Mol Cell Biol 10, 778–790.
Vogt DL, Gray CD, Young WS 3rd, Orellana SA, Malouf AT (2007). ARHGAP4 is a novel RhoGAP that mediates inhibition of cell motility and axon outgrowth. Mol Cell Neurosci 36, 332–342.
Weiner OD, Rentel MC, Ott A, Brown GE, Jedrychowski M, Yaffe MB, Gygi SP, Cantley LC, Bourne HR, Kirschner MW (2006). Hem-1 complexes are essential for Rac activation, actin polymerization, and myosin regulation during neutrophil chemotaxis. PLoS Biol 4, e38.
Wong K *et al*. (2001). Signal transduction in neuronal migration: roles of GTPase activating proteins and the small GTPase Cdc42 in the Slit-Robo pathway. Cell 107, 209–221.
Wu YI, Frey D, Lungu OI, Jaehrig A, Schlichting I, Kuhlman B, Hahn KM (2009). A genetically encoded photoactivatable Rac controls the motility of living cells. Nature 461, 104–108.
Yamazaki D, Kurisu S, Takenawa T (2009). Involvement of Rac and Rho signaling in cancer cell motility in 3D substrates. Oncogene 28, 1570–1583.
Yamazaki D, Suetsugu S, Miki H, Kataoka Y, Nishikawa S, Fujiwara T, Yoshida N, Takenawa T (2003). WAVE2 is required for directed cell migration and cardiovascular development. Nature 424, 452–456.
Yang Y, Marcello M, Endris V, Saffrich R, Fischer R, Trendelenburg MF, Sprengel R, Rappold G (2006). MEGAP impedes cell migration via regulating actin and microtubule dynamics and focal complex formation. Exp Cell Res 312, 2379–2393.